photonics

MDPI

Communication

Optical Temperature Sensors Based on Down-Conversion Nd^{3+},Yb^{3+}:$LiYF_4$ Microparticles

Anna Ginkel [1], Maksim Pudovkin [1,*], Ekaterina Oleynikova [1], Slella Korableva [1] and Oleg Morozov [1,2]

[1] Institute of Physics, Kazan Federal University, 18th Kremlyovskaya Street, 420008 Kazan, Russia
[2] Zavoisky Physical-Technical Institute, FRC Kazan Scientific Center of RAS, Sibirskii Ave., 10/7, 420029 Kazan, Russia
* Correspondence: jaz7778@list.ru

Abstract: Nd^{3+} (0.3 mol.%), Yb^{3+} (0, 1, 2, 3 and 5 mol.%): $LiYF_4$ phosphors were grown by the Bridgman–Stockbarger technique. The luminescence intensity ratio (LIR) of Nd^{3+} ($^4F_{3/2}$–$^4I_{9/2}$, ~866 nm) and Yb^{3+} emission ($^2F_{5/2}$–$^2F_{7/2}$, ~980 nm) was taken as a parameter. The energy exchange between $^4F_{3/2}$ (Nd^{3+}) and $^2F_{5/2}$ (Yb^{3+}) occurs via phonons, which elucidates the LIR temperature dependence. The influence of the cross-relaxation process on the temperature sensitivity was estimated as negligible. The LIR function depends on the Yb^{3+} concentration at a fixed 0.3 mol.% Nd^{3+}. The maximum S_a and S_r value were reached for Nd^{3+} (0.3%), Yb^{3+} (1.0%): $LiYF_4$ (S_a = 0.007 K^{-1} at 320 K) and Nd^{3+} (0.3%), Yb^{3+} (5.0%): $LiYF_4$ (S_r = 1, 1.03%*K^{-1} at 260 K), respectively.

Keywords: luminescent thermometry; down-conversion; optical temperature sensors

Citation: Ginkel, A.; Pudovkin, M.; Oleynikova, E.; Korableva, S.; Morozov, O. Optical Temperature Sensors Based on Down-Conversion Nd^{3+},Yb^{3+}:$LiYF_4$ Microparticles. *Photonics* **2023**, *10*, 375. https://doi.org/10.3390/photonics10040375

Received: 17 February 2023
Revised: 22 March 2023
Accepted: 25 March 2023
Published: 28 March 2023

1. Introduction

Currently, there is a rapid development of such branches of science and industry as circuitry, space and aviation industries, cell biology and theranostics. For these industries, there is an urgent need to measure the temperature fields of an object with submicron resolution. For some medical and scientific applications, non-contact or semi-contact temperature control methods with high spatial resolution are required [1,2]. An alternative method of temperature measurement is luminescent thermometry using phosphors having temperature-dependent luminescence parameters. Indeed, the ability to work in the UV, visible and near-IR spectral ranges, as well as nano-sized dimensionality of phosphors, provide submicron spatial resolution in temperature mapping. Here the phosphors serve as probes transmitting information about temperature over a distance through luminescence signal. In the case of temperature mapping of micro-circuit, the dielectric layer should be coated on its surface. In the case of hyperemia of the cell temperature mapping, the optical probes should be located in the special part of the studied object. For this application, some double-doped rare-earth inorganic phosphors demonstrate temperature-dependent spectral-kinetic properties due to temperature-dependent energy exchange processes between the doping ions [3,4]. A promising down-conversion ion pair is Nd^{3+}/Yb^{3+}. Particularly, the transfer of energy from $^4F_{3/2}$ (Nd^{3+}) level to $^2F_{5/2}$ (Yb^{3+}) one is accompanied by the emission of phonon [5]. The efficiency of such energy transfer depends on the temperature. This fact paves the way for the optical temperature measurement based on rare-earth double-doped phosphors. However, there is another interesting energy transfer process called cross-relaxation [6,7]. For example, cross-relaxation in the Nd^{3+},Yb^{3+}:$LiYF_4$ system is possible under Nd^{3+} excitation at 355 nm (($^2F_{7/2}$–$^2F_{5/2}$ (Yb^{3+}) and $^2K_{15/2}$/$^4G_{11/2}$–$^4F_{3/2}$ (Nd^{3+})). However, the contribution of the cross-relaxation in the temperature dependence of spectral-kinetic characteristics is still questionable. Indeed, the work [8] informs that resonant cross-relaxation processes in Ho^{3+}:$LiYF_4$ are independent of the temperature. Since the process of cross relaxation can proceed with the participation

of phonons, which makes this mechanism temperature dependent, with a tendency to decrease the influence of cross relaxation with decreasing temperature. However, there is a cross-relaxation process without the participation of phonons, with resonant energy transfer depending on the distance between the suitable energy levels [9,10]. To investigate this contribution, we studied spectral characteristics of Nd^{3+},Yb^{3+}:$LiYF_4$ microparticles at two different regimes of optical excitation (at 355 and 520 nm). The choice of $LiYF_4$ matrix is based on its low phonon energy (~140 to 570 cm^{-1}) [11,12] that provides higher quantum luminescence yield due to a decrease in the probability of multiphonon nonradiative relaxation [13]. Additionally, $LiYF_4$ ensures the Y^{3+} substitution without changing the valence [14]. For optical temperature sensing, essential characteristics of sensors are absolute and relative temperature sensitivities (S_a and S_r, respectively), which are determined in Ref. [2]. Indeed, Nd^{3+},Yb^{3+}:YF_3 (S_a = 0.002 K^{-1} at 150 K) [15], Nd^{3+},Yb^{3+}: YVO_4 (S_r = 0.085% K^{-1} at 183 K) [16] demonstrate a noticeable temperature sensitivity. Here, the luminescence intensity ratio (LIR) between the Nd^{3+} and Yb^{3+} emissions was chosen as temperature-dependent parameter. The choice of LIR is justified by the fact that LIR is independent of the fluctuations in the of the excitation irradiation power density on opposite to luminescence intensity parameter. Thus, LIR has a great advantage in terms of "luminescence intensity", which depends on the power density of the exciting radiation. In the case of comparison of up- and down-conversion, it should be noted, that up-conversion phosphors are studied deeper compared to down-conversion ones. Moreover, in such ion pair as Er/Yb, Pr/Yb, Tm/Yb temperature sensitivity is achieved because of the presence of thermally coupled electron levels. It seems that it is difficult to manipulate the electron level structure and as a consequence temperature sensitivity. On the other hand, temperature sensitivity of down-conversion phosphors is mostly based on phonon-assisted energy exchange processes between doping ions. There are more ways to optimize the impact of these processes on the temperature sensitivity via choosing concentration of both ions and choosing matrices [17–19], In the case of matrix choice, fluoride matrices seem to be very promising compared to oxide ones due to low phonon energy that leads to the decrease in multiphonon relaxation probability. On the other hand, the Nd^{3+}/Yb^{3+} ion pair is very specific due to relatively large difference in ionic radii. Since the Nd^{3+} concentration was demonstrated to be low (0.1–0.5%) and Yb^{3+} concentration should be notably higher (up to 10%) [18], the main requirements are imposed on the matrix ion that is expected to be substituted by Yb^{3+} ion in order to create suitable concentration without miro-strains and double-phase formation. Here Y^{3+} based matrices seem to be very promising. Such matrix, as YF_3 demonstrates undesirable broad emission related to the presence of specific defects under UV excitation [15,20]. In its turn, $LiYF_4$ is free from such peculiarities [21].

The objective of this work was to reveal the impact of excitation conditions on temperature sensitivity of Nd^{3+},Yb^{3+}:$LiYF_4$ phosphors.

2. Materials and Methods

Powders of LiF (99.999% purity, Lanhit, Russia), YF_3 (99.999% purity, Lanhit, Russia), NdF3 (99.999% purity, Lanhit, Russia) and YbF_3 (99.999% purity, Lanhit, Russia) fluorides were used as initial materials. The YF_3, NdF_3 and YbF_3 components were previously dried for 5 h at 100°C in vacuum. Then they were purified and fluorinated with 2 wt% PbF_2 for 5 h in vacuum at 900 °C and then were held for 2h in vacuum at a temperature above the corresponding melting points. Crystal growth process was carried out in a vacuum (~10–5–10–6 mbar) in a graphite crucible on a seed. The crystals were grown from the melt by vertical technique of Bridgman–Stockbarger. The temperature gradient at the solid-liquid interface was in the 85–100 °C/cm range. The pulling rate was chosen as 1 mm/h. The crystal size was 16 mm in length and 6 mm in diameter. A plate 2 mm thick was cut from the lower part of the grown crystal and was milled in the agate mortar into powder [19]. The phase composition was studied by X-ray diffraction (XRD) using a Shimadzu XRD-7000S X-ray diffractometer (Cu K_α radiation λ = 0.15406 nm). The luminescence spectra were detected via a CCD spectrometer "StellarNet" having spectral resolution of 0.5 nm. The

luminescence measurements were acquired using JV LOTIS TII laser system (420–1200 nm range, model LS-2134UTF) at 520 nm in the 80–320 K temperature range (λ_{ex} = 520 nm and 355 nm, corresponds to $^4I_{9/2}$–$^2K_{13/2}/^2G_{9/2}$ and $^4I_{9/2}$–$^4D_{5/2}$, absorption bands of Nd^{3+} ions, respectively). The measurements were carried out in the temperature range from 80 to 320 K. The temperature controlling was carried out via "CRYO industries" cooler equipped with LakeShore Model 325 temperature controller. The liquid nitrogen was utilized as a cooler. The pulse width and the rate of the pulse repetition were 10 ns and 10 Hz, respectively. Pulse laser irradiation was taken in order to exclude heating of the sample. The principal experimental set-up is represented in Figure S1 (Supplementary).

3. Results and Discussion

The sample phase composition was confirmed via method of X-ray diffraction (XRD). In particular, the XRD pattern of the Nd^{3+} (0.3 mol.%),Yb^{3+}(1.0 mol.%):$LiYF_4$ sample is shown in Figure 1.

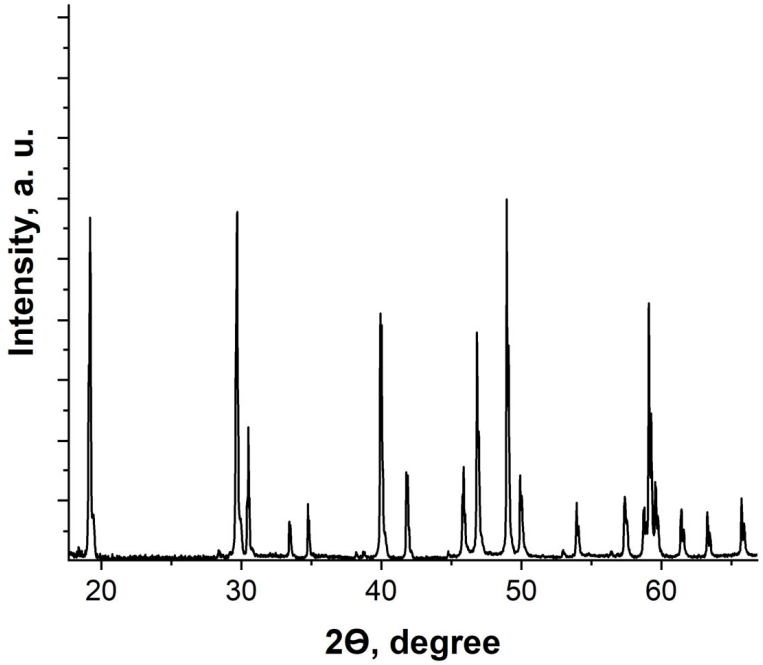

Figure 1. XRD patterns of Nd^{3+} (0.3%), Yb^{3+} (2.0%): $LiYF_4$ phosphors.

The X-ray diffraction pattern is consistent with the literature data [22] and corresponds to the trigonal structure of $LiYF_4$. The well-defined $LiYF_4$ peaks, the absence of impurity and amorphous phases are clearly seen. The Figure 2 demonstrates a simplified energy level diagram as well as main energy transfer processes [5]. These energy transfer processes involve $^4F_{3/2}$ (Nd^{3+}) and/or $^2F_{5/2}$ (Yb^{3+}) levels.

Particularly, under 355 nm excitation ($^4I_{9/2}$–$^4D_{5/2}$ absorption band of Nd^{3+}) the $^4F_{3/2}$ level of Nd^{3+} in populated via cross-relaxation ($^2F_{7/2}$–$^2F_{5/2}$ (Yb^{3+}) and $^2K_{15/2}$–$^4F_{3/2}$ (Nd^{3+})), radiative and nonradiative transitions from the higher energy levels. In turn, excitation at 520 nm ($^4I_{9/2}$–$^2K_{13/2}/^2G_{9/2}$ absorption band of Nd^{3+}) excluded cross-relaxation process. Indeed, in order to confirm the presence of radiative and nonradiative transitions, we detected the luminescence spectrum of Nd^{3+} (0.3 mol.%) Yb^{3+} (2 mol.%):$LiYF_4$ phosphors in the slightly broader (spectral range 710–1100 nm) spectral range under 355 nm excitation (Figure 3). According to the literature data [5], there were two peaks at ~740 and 800 nm that were interpreted as transitions from the upper $^4D_{5/2}$ and $^4P_{3/2}$ levels to ^4F_J of Nd^{3+}. Hence, the ^4F_J levels were populated via these radiative transitions. The nonradiative transitions between the ^4F_J levels were also possible and the population of the lowest $^4F_{3/2}$ level could also be nonradiative (for example from $^4F_{7/2}$).

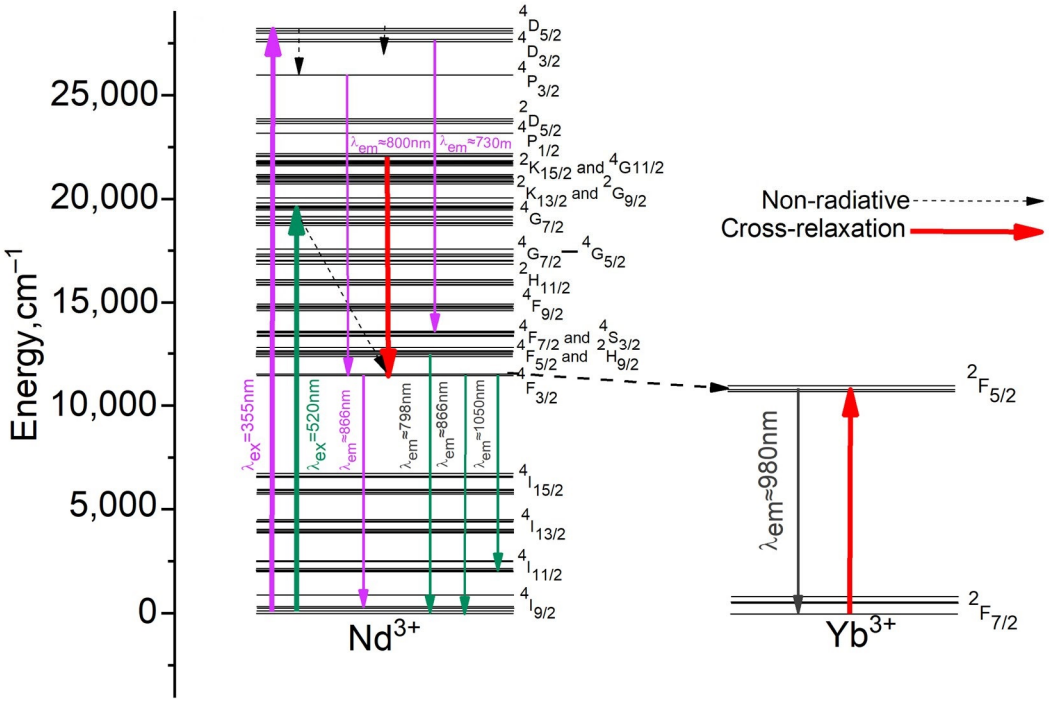

Figure 2. An energy level diagram of Nd^{3+}, Yb^{3+} system.

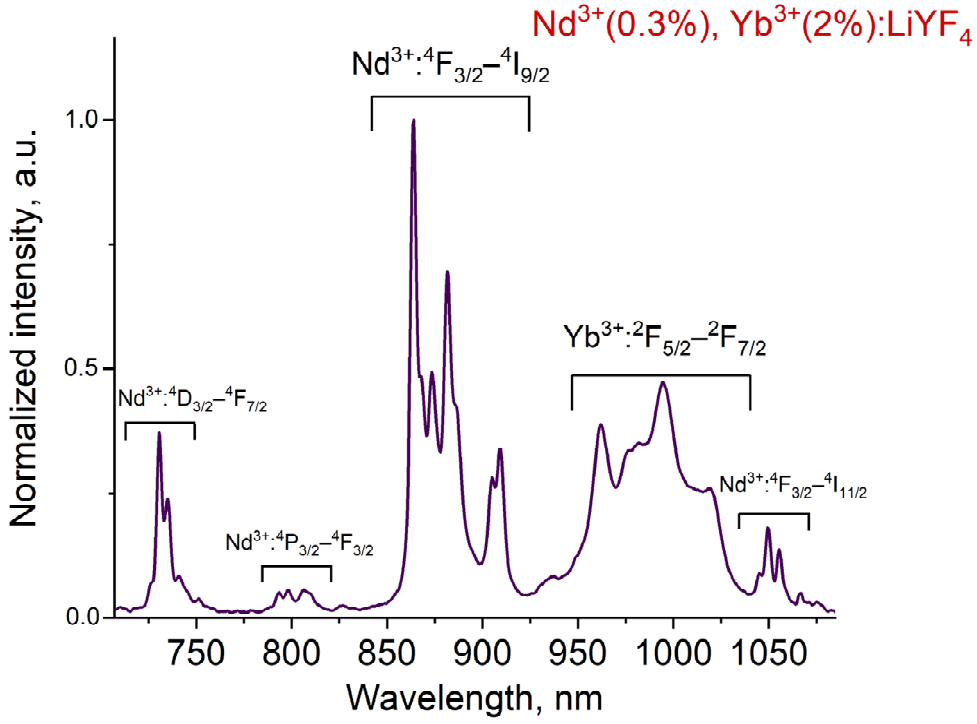

Figure 3. The room temperature spectrum of Nd^{3+} (0.3%), Yb^{3+} (2.0%): $LiYF_4$ phosphors normalized at 866 nm. The excitation λ_{ex} = 355 nm corresponds to $^4I_{9/2}$–$^4D_{5/2}$ of Nd^{3+} absorption band. The spectrum illustrates the presence of $^4D_{5/2}$, $^4P_{3/2}$–^4F_J transitions.

Normalized luminescence spectra of Nd^{3+} (0.3%), Yb^{3+} (1.0–5.0 mol.%):$LiYF_4$ phosphors detected at room temperature are shown in Figure 4. Excitation of the system was carried out at λ_{ex} = 520 nm, ($^2K_{13/2}$–$^2G_{9/2}$, absorption band of Nd^{3+} ions). The observed Yb^{3+} luminescence indicates the energy transfer from Nd^{3+} to Yb^{3+}. All peaks were identi-

fied as the transitions from $^4F_{3/2}$ (Nd^{3+}) and $^2F_{5/2}$ (Yb^{3+}) to the lower energy levels. The peaks had a complex structure because of the complicated Stark structure of the electron levels. The emission intensity of Yb^{3+} rises with the increase in Yb^{3+} concentration compared to Nd^{3+} emission intensity. These processes of the energy transfer involve $^4F_{3/2}$ (Nd^{3+}) and $^2F_{5/2}$ (Yb^{3+}).

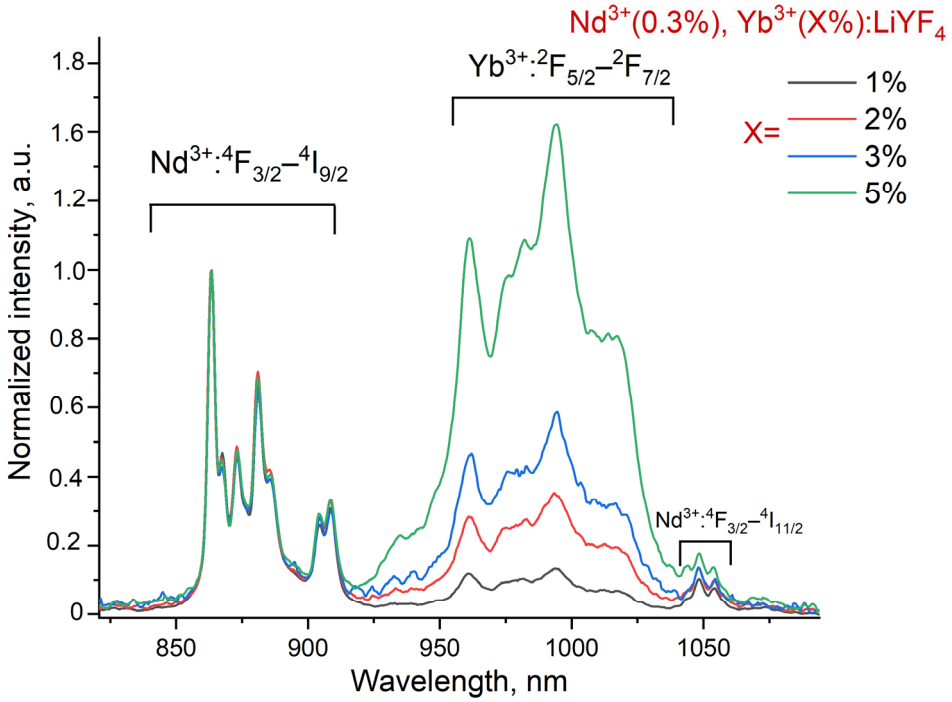

Figure 4. Normalized luminescence spectra of Nd^{3+} (0.3%), Yb^{3+} (1.0, 2.0, 3.0, and 5.0%):$LiYF_4$ phosphors recorded at room temperature. The excitation λ_{ex} = 520 nm corresponds to $^4I_{9/2}$–$^2K_{13/2}$/$^2G_{9/2}$ of Nd^{3+} absorption band. The spectra are normalized at ~861 nm peak of Nd^{3+}.

According to ref. [18], the energy transfer between doping ions can be described by a process characterized by its probabilities. Energy exchange process between Nd^{3+} ions seemed to be also probable; however, the Nd^{3+} (0.3 mol.%) concentration for the studied samples did not change, its effect on the studied temperature-dependent luminescent properties was assumed to be negligible. Additionally, in ref [19,23], a cross-relaxation process was proposed for the Nd^{3+}/Yb^{3+} pair. This process involves the Nd^{3+} ($^2K_{15/2}$/$^4G_{11/2}$–$^4F_{3/2}$) and Yb^{3+} ($^2F_{7/2}$–$^2F_{5/2}$) transitions. The room temperature luminescence decay curves of the $^4F_{3/2}$–$^4I_{9/2}$ transition (866 nm) of Nd^{3+} under 355 nm excitation are shown in Figure 5a.

As we can see, with an increase in the Yb^{3+} concentration, the Nd^{3+} luminescence lifetime decreased, which indicates an energy transfer from Nd^{3+} to Yb^{3+}. In addition, as mentioned above, the additional population of Nd^{3+} and Yb^{3+} levels may be related to cross-relaxation. Indeed, the luminescence rising time curve at an excitation wavelength of 355 nm are seen in Figure 5a. The luminescence rising time was shortened with an increase in Yb^{3+} concentration; this process of shortening of the luminescence rising time curves indicates cross-relaxation. Indeed, the cross-relaxation was notably faster compared to radiative transitions from higher levels to $^4F_{3/2}$ one. Indeed, the work [24] estimated time resonant cross-relaxation between Tm^{3+} ions from 8 μs (at 1.0% concentration) to 30 μs (at 4.0 % concentration). The contribution of faster cross-relaxation process in population of $^4F_{3/2}$ level increased with the increase in Yb^{3+} that led to rising-time shortening. Figure 5b shows the luminescence decay time at an excitation wavelength of 520 nm as a function of Yb^{3+} concentration. We can observe the same tendency for the decay curves. However, the rising time curves are not observed, hence, we excluded the cross-relaxation process by

using 520 nm excitation regime. It can also be seen that cross-relaxation was impossible for 520 nm photons, as they had too low energy (Figure 2).

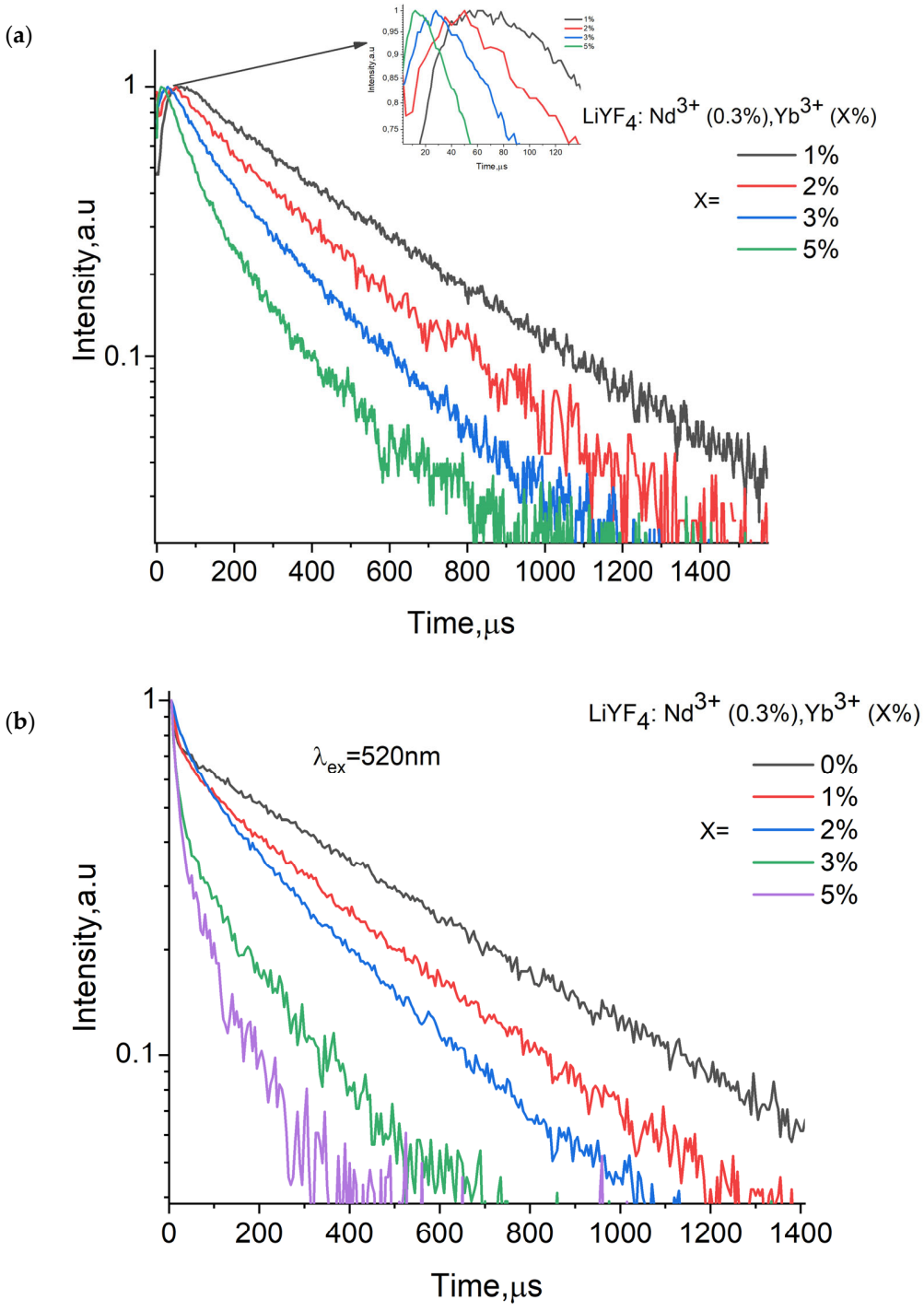

Figure 5. (**a**). Normalized room temperature lifetime curves of $^4F_{3/2}$–$^4I_{9/2}$ emission of Nd^{3+} (at 866 nm) in Nd^{3+} (0.5%), Yb^{3+} (1, 2, 3, and 5%):$LiYF_4$ phosphors. The excitation wavelength λ_{ex} = 355 nm corresponds to $^4I_{9/2}$–$^4D_{5/2}$ absorption band of Nd^{3+}. The inset demonstrates the luminescence rising time as a function of the Yb^{3+} concentration. (**b**). Normalized room temperature lifetime curves of $^4F_{3/2}$–$^4I_{9/2}$ emission of Nd^{3+} (at 866 nm) in Nd^{3+} (0.5%), Yb^{3+} (0, 1, 2, 3, and 5%):$LiYF_4$ phosphors. The excitation wavelength λ_{ex} = 520 nm corresponds to $^4I_{9/2}$–$^2K_{13/2}/^2G_{9/2}$ absorption band of Nd^{3+}.

It was important to ensure that the samples were not heated up by the excitation irradiation. We selected the well suited excitation power densities according to [15]. The temperature evolution of the normalized luminescence spectra of Nd^{3+} (0.5%), Yb^{3+} (2.0%):$LiYF_4$ in the 80–320 K range is shown in Figure 6. It can be seen that the relative intensities of the Nd^{3+} and Yb^{3+} emission peaks depended on the temperature for all samples. In order to investigate this spectral temperature-dependence, the luminescence intensity ratio (LIR) was calculated according to the common Equation (1). The LIR values were carried out in the wavelength range of 842–922 nm (Nd^{3+}) and 936–1037 nm (Yb^{3+}) for both 355 and 520 nm excitations.

$$\mathrm{LIR(Y)} = \frac{\int \mathrm{I_{Nd}}(\lambda, \mathrm{T})\mathrm{d}\lambda}{\int \mathrm{I_{Yb}}(\lambda, \mathrm{T})\mathrm{d}\lambda} \quad (1)$$

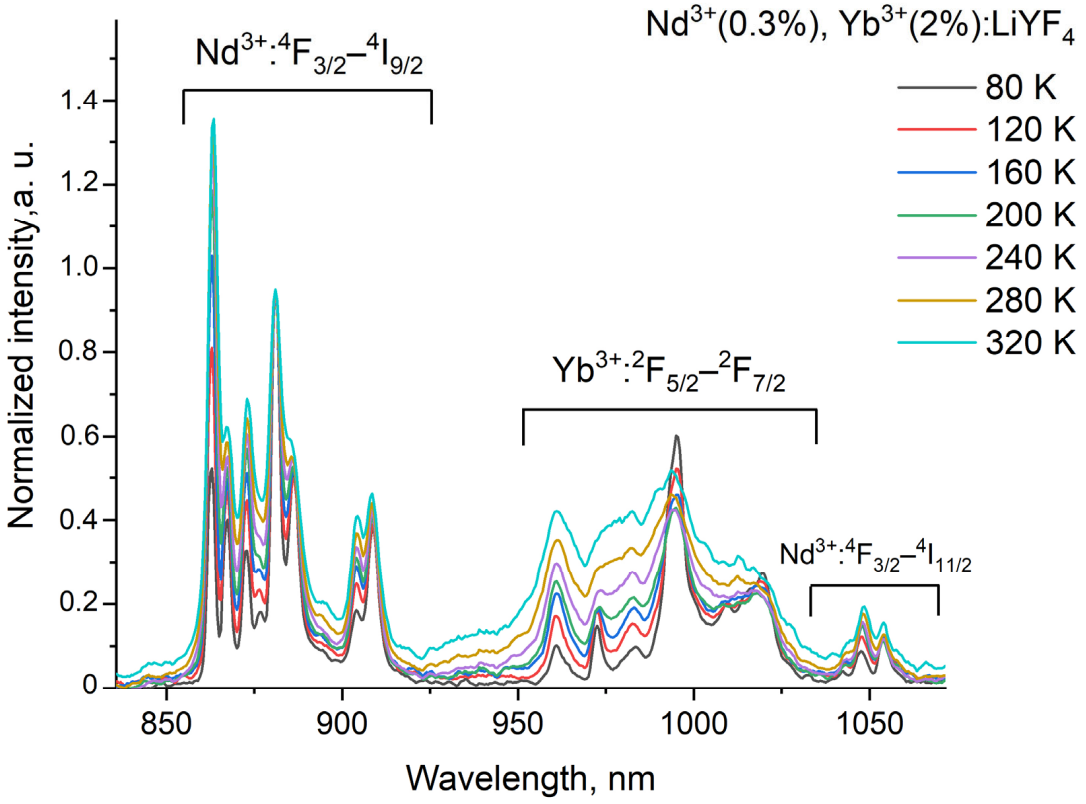

Figure 6. The normalized at 881 nm Nd^{3+} (0.3%), Yb^{3+} (2.0%):$LiYF_4$ luminescence spectra recorded in the 80–320 K range. The excitation λ_{ex} = 520 nm corresponds to $^4I_{9/2}$–$^2K_{13/2}$/$^2G_{9/2}$ absorption band of Nd^{3+}.

The LIR dependences are presented in Figure 7. It is clearly seen that the shape of the LIR functions demonstrated weak dependence on the concentration of Yb^{3+} at a constant 0.3 mol.% of Nd^{3+}. The LIR function had complex temperature dependence with segments of an increase in the range of 77–220 K, as well as a decrease character in the range of 230–320 K. This dependence was most pronounced for 1 mol.% Yb^{3+}. Based on the fact that the nature of the change in the LIR function also depended on the processes of energy transfer between two ions, there is a possibility that cross-relaxation influenced the character of the change in the LIR curves. The LIR functions of the Nd^{3+} (0.3%), Yb^{3+} (1.0–5.0 mol.%):$LiYF_4$ samples had complicated shape with growth part in the temperature range of 75–200 K and a decay part in the temperature range of 200–320 K. The growing character of the LIR function takes place because Nd^{3+} intensity increases faster that Yb^{3+} one with temperature. It occurred because the phonon appearance probability is relatively low in this temperature range. Then, this probability increased and the population of

$^2F_{5/2}$ level of Yb^{3+} happened more efficiently and the intensity of Yb^{3+} started to grow, in turn the efficiency of depopulation of $^4F_{3/2}$ level of Nd^{3+} also increased and I_{Nd}/I_{Yb} started to decay with the temperature increase. Figure 8 shows the LIR curves at different excitation wavelengths of 355 and 520 nm for the sample Nd^{3+} (0.3%), Yb^{3+} (2%): $LiYF_4$. As we can see in the Figure 8, the shape of the LIR curves as a function of temperature is independent of excitation wavelengths. To quantitatively compare both functions, we represented the parameters of fitting procedure in Table S1 of Supplementary File. The parameters are very close to each other. This may tell us that the population of the Yb^{3+} level due to the cross-relaxation process does not notably affect the temperature sensitivity and the efficiency of cross-relaxation does not depend on temperature. However, it is worth considering that the same LIR value was achieved for two different temperatures for 120 and 280 K. It is worth considering that temperature measurement for this class of substances was possible from 200 K., which is suitable for measurements in fundamental biology, circuitry, etc. [25].

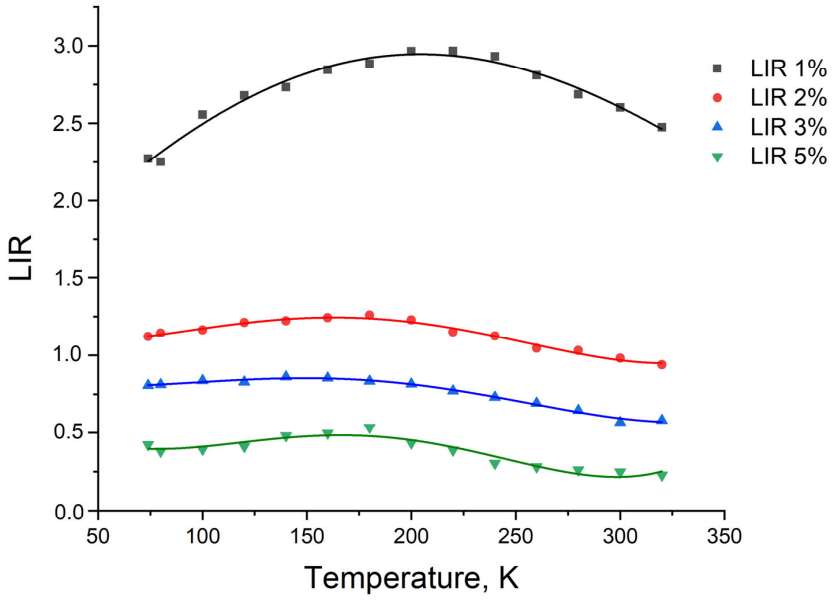

Figure 7. The LIR curves for I (Nd^{3+}, $^4F_{3/2}$–$^4I_{9/2}$, ~866 nm) and I (Yb^{3+}, $^2F_{5/2}$–$^2F_{7/2}$, ~980 nm) luminescence peaks.

In order to strengthen the argument of the low temperature dependence of cross-relaxation in the studied system, we performed kinetic characterization of the studied samples in the 80–320 K range. Indeed, the presence of rising time curve for $^4F_{3/2}$–$^4I_{9/2}$ peak at 355 nm excitation was related to non-resonant excitation. The $^4F_{3/2}$ is populated via transitions from the higher levels that have their own lifetime of the exited state. Thus, rising time was determined by the rate of transitions from higher levels as well as the rate of cross-relaxation [19,26]. If the rising time depends on temperature, hence, one or both above-mentioned processes are temperature dependent. The results of kinetic characterization of Nd^{3+} (0.3%), Yb^{3+} (2.0%):$LiYF_4$ sample under 355 nn excitation are represented in Figure 9.

It can be seen that rising time did not demonstrate clear temperature dependence. The obtained results are an argument for the low temperature dependence of cross-relaxation process at least in the precent temperature range. It can also be observed that in the 80–200 K range, the decay curves were almost the same and in the higher temperature range the decay time decreased with the increase in temperature. This phenomenon cab be explained by the fact that the energy transfer between $^4F_{3/2}$ (Nd^{3+}) and $^2F_{5/2}$ (Yb^{3+}) was phonon-assisted and the probability of phonon appearance increased with the temperature increase.

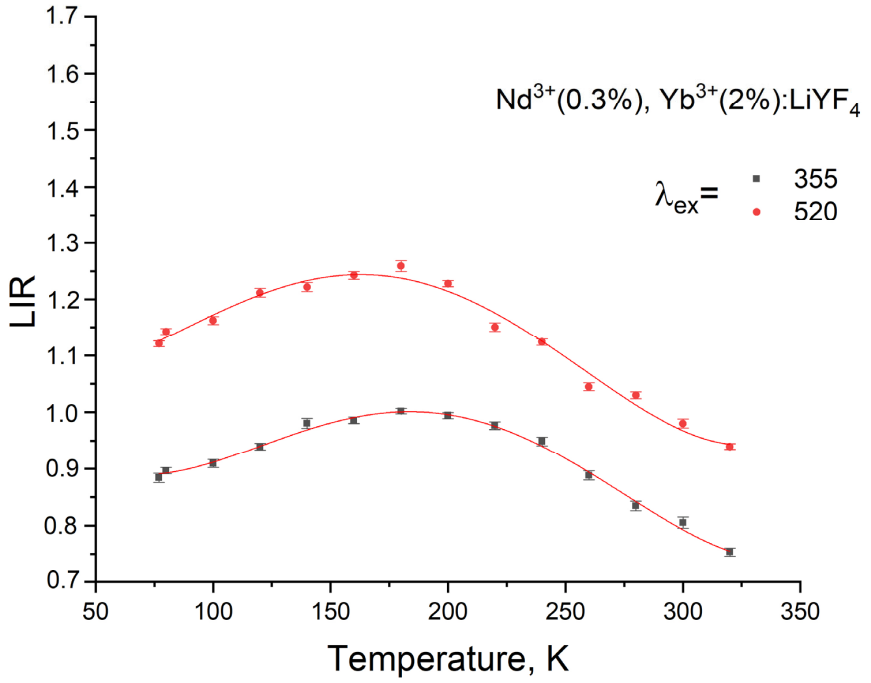

Figure 8. The LIR curves of both I(Nd^{3+}, $^4F_{3/2}$–$^4I_{9/2}$, ~866 nm) and I (Yb^{3+}, $^2F_{5/2}$–$^2F_{7/2}$, ~980 nm) luminescence peaks at different excitation wavelengths λex = 520 nm and λex = 355 nm.

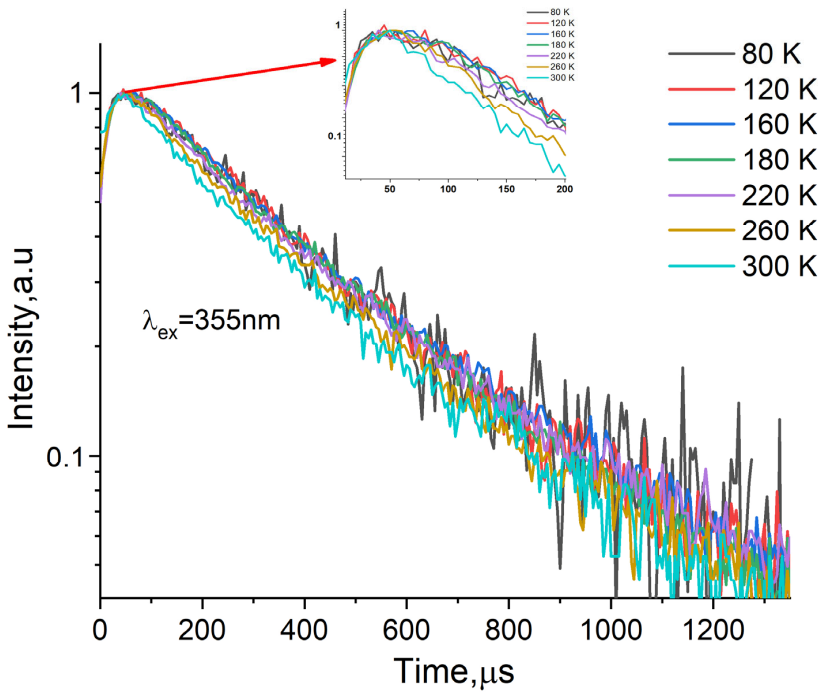

Figure 9. Lifetime curves of Nd^{3+} (0.3%), Yb^{3+} (2.0%):$LiYF_4$ sample under 355 nm excitation in the 80–320 K range.

For temperature mapping instrumentation, the absolute S_a and relative temperature sensitivity S_r are very crucial performances. The S_a [K^{-1}] and S_r [%*K^{-1}] are determined as [2,27]:

$$S_a = \frac{d(LIR)}{dT} \quad (2)$$

$$S_r = \frac{1}{LIR}\left|\frac{d(LIR)}{dT}\right| * 100\% \quad (3)$$

The S_r and S_a curves for all the samples are represented in Figure 10a,b, respectively. The maximum S_a value is achieved for Nd^{3+} (0.3%), Yb^{3+} (1.0%):$LiYF_4$ (S_a = 0.007 K^{-1} at 320 K). The rest of the samples demonstrate notably lower values of S_a. The maximum S_r value is achieved for Nd^{3+} (0.3%), Yb^{3+} (5.0%):$LiYF_4$ (S_r = 1.03%*K^{-1} at 260 K). The S_a and S_r values of the studied samples are compared to the counterparts in Table 1. Our samples demonstrate competing values compared to the temperature sensitivity values for these substances.

(**a**)

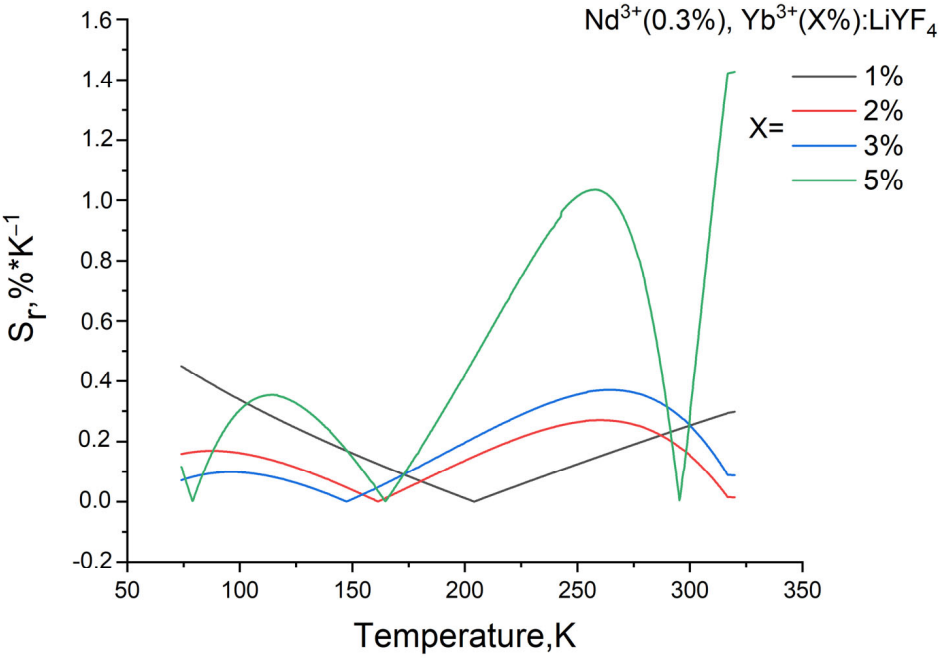

(**b**)

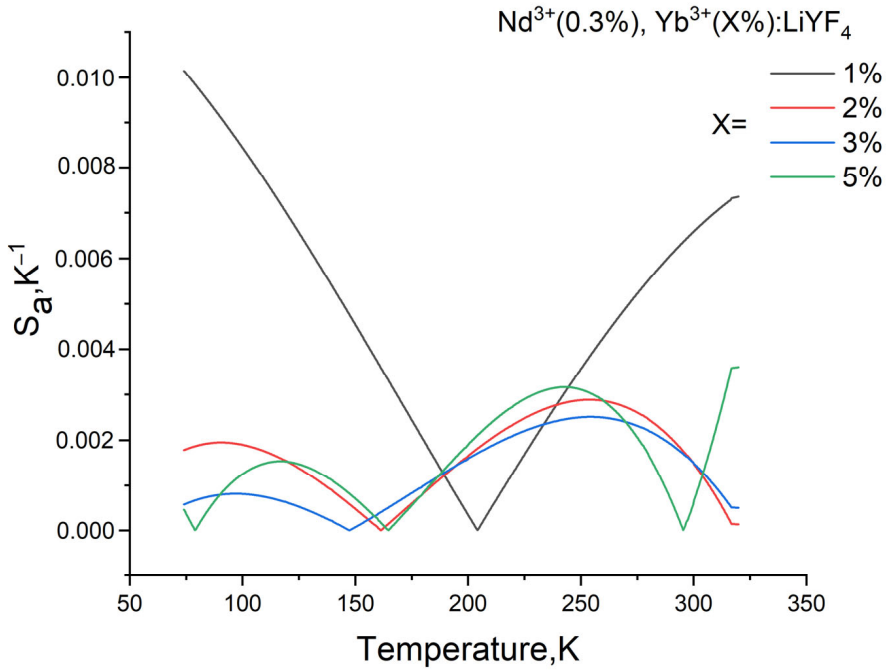

Figure 10. (**a**) Relative temperature sensitivity (S_r) and (**b**) absolute temperature sensitivity (S_a) as a function of temperature for Nd^{3+}, Yb^{3+}:$LiYF_4$ samples.

Table 1. The performances of rare-earth doped optical thermometers.

Sample	Transitions, Detected Wavelengths, and Conditions of the Excitation	Maximum S_a [K^{-1}]	Maximum S_r [%/K]	T,K	Ref.
$Tb_{0.99}Eu_{0.01}(BDC)_{1.5}(H_2O)_2$	Eu^{3+} ($^5D_0$–$^7F_2$), Tb^{3+} ($^5D_4$–$^7F_5$) λ_{ex} = 320 nm	-	0.14	283–333	[28]
$LiYF_4$: Nd^{3+}, Yb^{3+}	Nd^{3+} ($^4F_{3/2}$–$^4I_{9/2}$), Yb^{3+} ($^4F_{5/2}$–$^2F_{7/2}$), λ_{ex} = 520 nm	0.007	1.03	240–320	This work
$SrTiO_3$:Ni^{2+},Er^{3+}	Er^{3+} ($^4I_{13/2} \rightarrow {}^4I_{15/2}$) Ni^{2+} ($^3T_{2g}(F) \rightarrow {}^3A_{2g}(F)$), λ_{ex} = 375 nm	-	0.76	303	[29]
YVO_4:Nd^{3+}	Nd^{3+} ($^4F_{3/2}$–$^4I_{11/2}$) λ_{ex} = 808 nm	-	0.46	323	[16]
PrP_5O_{14}	Pr^{3+} ($^3P_0 \rightarrow {}^1D_2$) λ_{ex} = 488 nm	-	0.46	363	[30]
$NaPr(PO_3)_4$	Pr^{3+} ($^3P_0$ –$^3H_6$) λ_{ex} = 488 nm	0.0043	-	300–365	[30]
LaF_3:Nd^{3+}	Nd^{3+} ($^4F_{3/2}$ -$^4I_{9/2}$) λ_{ex} = 808 nm	-	0.1	293	[31]
MOF: Eu^{3+} /Tb^{3+}	Tb^{3+} ($^5D_4 \rightarrow {}^7F_5$) and Eu^{3+} ($^5D_0 \rightarrow {}^7F_2$) λ_{ex} = 340 nm	-	0.57	150–300	[32]
YF_3: Nd^{3+}, Yb^{3+}	Nd^{3+} ($^4F_{5/2}$–$^4I_{11/2}$) λ_{ex} = 790 nm	0.64	0.92	100	[33]
$NaYbF_4$: Nd@$NaYF_4$: Nd	Nd^{3+} ($^4F_{5/2}$–$^4I_{11/2}$) λ_{ex} = 790 nm	0.7		300	[34]

4. Conclusions

Potential optical temperature sensors based on Nd^{3+} (0.3 mol.%), Yb^{3+} (1.0, 2.0, 4.0, and 5.0 mol.%):$LiYF_4$ phosphors were studied in the 80–320 K range. It was found that the LIR function depends on the Yb^{3+} concentration at a fixed 0.3 mol.% of Nd^{3+}. The LIR functions were studied at different excitation wavelengths at 355 and 520 nm. It was shown that the cross-relaxation does not have a notable impact on the temperature sensitivity of the spectral characteristics of the samples. The maximum value of S_a is achieved for Nd^{3+} (0.3%), Yb^{3+} (1.0%): $LiYF_4$ (S_a = 0.007 K^{-1} at 320 K) and S_r Nd^{3+} (0.3%), Yb^{3+} (5.0%): $LiYF_4$ (S_r = 1.03%*K^{-1} at 260 K).

Supplementary Materials: The following supporting information can be downloaded at: https://www.mdpi.com/article/10.3390/photonics10040375/s1. Figure S1. Experimental set-up. 1 and 4 are lenses, 2 and 3 are crio-system and the sample, 5–optical filter, 6–waveguide, 7–spectrometer, 8–PC. Table S1. Polynomal parameters for LIR

Author Contributions: A.G.: investigation, data curation, writing—original draft, M.P.: conceptualization, investigation, resources, writing—original draft, E.O.: investigation, S.K.: investigation, O.M.: investigation. All authors have read and agreed to the published version of the manuscript.

Funding: The study was funded by the grant from the Russian Science Foundation number 22-72-00129, https://rscf.ru/project/22-72-00129/ (accessed on 1 August 2022).

Institutional Review Board Statement: Not applicable.

Informed Consent Statement: Not applicable.

Data Availability Statement: Not applicable.

Conflicts of Interest: The authors declare no conflict of interest.

References

1. Cai, T.; Li, Y.; Guo, S.; Peng, D.; Zhao, X.; Liu, Y. Pressure effect on phosphor thermometry using Mg_4FGeO_6: Mn. *Meas. Sci. Technol.* **2019**, *30*, 027001. [CrossRef]
2. Brites, C.D.; Balabhadra, S.; Carlos, L.D. Lanthanide-based thermometers: At the cutting-edge of luminescence thermometry. *Adv. Opt. Mater.* **2019**, *7*, 1801239. [CrossRef]
3. Zhuang, Y.; Wang, D.; Yang, Z. Upconversion luminescence and optical thermometry based on non-thermally-coupled levels of $Ca_9Y(PO_4)_7$: Tm^{3+}, Yb^{3+} phosphor. *Opt. Mater.* **2022**, *126*, 112167. [CrossRef]
4. Khadiev, A.R.; Korableva, S.L.; Ginkel, A.K.; Morozov, O.A.; Nizamutdinov, A.S.; Semashko, V.V.; Pudovkin, M.S. Down-conversion based Tm^{3+}: LiY_1-$XYbXF_4$ temperature sensors. *Opt. Mater.* **2022**, *134*, 113118. [CrossRef]
5. Maijer, J.M.; Aarts, L.; Ende, B.M.V.; Vlugt, T.J.H.; Maeijerink, A. Down conversion for solar cells in YF_3: Nd^{3+}, Yb^{3+}. *Phys. Rev. B* **2010**, *81*, 035107–035116. [CrossRef]

6. Sun, J.; Sun, Y.; Cao, C.; Xia, Z.; Du, H. Near-infrared luminescence and quantum cutting mechanism in $CaWO_4$: Nd^{3+}, Yb^{3+}. *Appl. Phys. B* **2013**, *111*, 367–371. [CrossRef]
7. Costa, F.B.; Yukimitu, K.; Nunes, L.A.D.O.; Figueiredo, M.D.S.; Silva, J.R.; Andrade, L.H.D.C.; Lima, S.M.; Moraes, J.C.S. High $Nd^{3+} \rightarrow Yb^{3+}$ energy transfer efficiency in tungsten-tellurite glass: A promising converter for solar cells. *J. Am. Ceram. Soc.* **2017**, *100*, 1956–1962. [CrossRef]
8. Gomes, L.; Courrol, L.C.; Tarelho, L.V.G.; Ranieri, I.M. Cross-relaxation process between +3 rare-earth ions in $LiYF_4$ crystals. *Phys. Rev. B* **1996**, *54*, 3825. [CrossRef]
9. Hegarty, J.; Huber, D.L.; Yen, W.M. Fluorescence quenching by cross relaxation in LaF_3: Pr^{3+}. *Phys. Rev. B* **1982**, *25*, 5638. [CrossRef]
10. Van Wijngaarden, J.T.; Scheidelaar, S.; Vlugt, T.J.H.; Reid, M.F.; Meijerink, A. Energy transfer mechanism for downconversion in the (Pr^{3+}, Yb^{3+}) couple. *Phys. Rev. B* **2010**, *81*, 155112. [CrossRef]
11. Miller, S.A.; Rast, H.E.; Caspers, H.H. Lattice vibrations of $LiYF_4$. *J. Chem. Phys.* **1970**, *52*, 4172–4175. [CrossRef]
12. Semashko, V.V.; Korableva, S.L.; Fedorov, P.P. Lithium Rare-Earth Fluorides as Photonic Materials: 2. Some Physical, Spectroscopic, and Lasing Characteristics. *Inorg. Mater.* **2022**, *58*, 447–492. [CrossRef]
13. Charfi, B.; Damak, K.; Alqahtani, M.S.; Hussein, K.I.; Alshehri, A.M.; Elkhoshkhany, N.; Assiri, A.L.; Alshehri, K.F.; Reben, M.; Yousef, E.S. Luminescence and Gamma Spectroscopy of Phosphate Glass Doped with Nd^{3+}/Yb^{3+} and Their Multifunctional Applications. *Photonics* **2022**, *9*, 406. [CrossRef]
14. Fedorov, P.P.; Semashko, V.V.; Korableva, S.L. Lithium rare-earth fluorides as photonic materials: 1. Physicochemical characterization. *Inorg. Mater.* **2022**, *58*, 223–245. [CrossRef]
15. Pudovkin, M.S.; Ginkel, A.K.; Lukinova, E.V. Temperature sensitivity of Nd^{3+}, Yb^{3+}: YF_3 ratiometric luminescent thermometers at different Yb^{3+} concentration. *Opt. Mater.* **2021**, *119*, 111328. [CrossRef]
16. Marciniak, L.; Bednarkiewicz, A.; Trejgis, K.; Maciejewska, K.; Elzbieciak, K.; Ledwa, K. Enhancing the sensitivity of a Nd^{3+}, Yb^{3+}: YVO_4 nanocrystalline luminescent thermometer by host sensitization. *Phys. Chem. Chem. Phys.* **2019**, *21*, 10532–10539. [CrossRef]
17. Wang, X.; Liu, Q.; Bu, Y.; Liu, C.S.; Liu, T.; Yan, X. Optical temperature sensing of rare-earth ion doped phosphors. *Rsc Adv.* **2015**, *5*, 86219–86236. [CrossRef]
18. Bednarkiewicz, A.; Stefanski, M.; Tomala, R.; Hreniak, D.; Strek, W. Near infrared absorbing near infrared emitting highly-sensitive luminescent nanothermometer based on Nd^{3+} to Yb^{3+} energy transfer. *Phys. Chem. Chem. Phys.* **2015**, *17*, 24315–24321.
19. Pudovkin, M.S.; Ginkel, A.K.; Morozov, O.A.; Kiiamov, A.G.; Kuznetsov, M.D. Highly-sensitive lifetime optical thermometers based on Nd^{3+}, Yb^{3+}: YF_3 phosphors. *J. Lumin.* **2022**, *249*, 119037. [CrossRef]
20. Santos, H.D.A.; Novais, S.M.V.; Jacinto, C. Optimizing the Nd: YF_3 phosphor by impurities control in the synthesis procedure. *J. Lumin.* **2018**, *201*, 156–162. [CrossRef]
21. Pudovkin, M.S.; Korableva, S.L.; Koryakovtseva, D.A.; Lukinova, E.V.; Lovchev, A.V.; Morozov, O.A.; Semashko, V.V. The comparison of Pr^{3+}: LaF_3 and Pr^{3+}: $LiYF_4$ luminescent nano-and microthermometer performances. *J. Nanoparticle Res.* **2019**, *21*, 266. [CrossRef]
22. Hu, J.; Xia, H.; Hu, H.; Zhang, Y.; Jiang, H.; Chen, B. Synthesis and efficient near-infrared quantum cutting of Pr^{3+}/Yb^{3+} co-doped $LiYF_4$ single crystals. *J. Appl. Phys.* **2012**, *112*, 073518. [CrossRef]
23. Bian, X.; Shi, Q.; Wang, L.; Tian, Y.; Xu, B.; Mamytbekov, Z.K.; Huang, P. Near-infrared luminescence and energy transfer mechanism in K_2YF_5: Nd^{3+}, Yb^{3+}. *Mater. Res. Bull.* **2019**, *110*, 102–106. [CrossRef]
24. Zheng, L.; Wu, H.; Zhang, L.; Luo, Y.; Pan, G.H.; Wang, X.J.; Hao, Z.; Zhang, J. Determination of cross-relaxation efficiency based on spectroscopy in thulium-doped rare-earth sesquioxides. *Ceram. Int.* **2023**, *49*, 11060–11066. [CrossRef]
25. Ximendes, E.C.; Santos, W.Q.; Rocha, U.; Kagola, U.K.; Sanz-Rodríguez, F.; Fernández, N.; Gouveia-Neto, A.D.S.; Bravo, D.; Domingo, A.M.; Rosal, B.D.; et al. Unveiling in vivo subcutaneous thermal dynamics by infrared luminescent nanothermometers. *Nano Lett.* **2016**, *16*, 1695–1703. [CrossRef]
26. Berdowski, P.A.M.; Lammers, M.J.J.; Blasse, G. $^5D_3$-$^5D_4$ cross-relaxation of Tb^{3+} in α-GdOF. *Chem. Phys. Lett.* **1985**, *113*, 387–390. [CrossRef]
27. Zhao, Y.; Wang, X.; Zhang, Y.; Li, Y.; Yao, X. Optical temperature sensing of up-conversion luminescent materials: Fundamentals and progress. *J. Alloy. Compd.* **2020**, *817*, 152691. [CrossRef]
28. Cadiau, A.; Brites, C.D.; Costa, P.M.; Ferreira, R.A.; Rocha, J.; Carlos, L.D. Ratiometric nanothermometer based on an emissive Ln^{3+}-organic framework. *ACS Nano* **2013**, *7*, 7213–7218. [CrossRef] [PubMed]
29. Matuszewska, C.; Elzbieciak-Piecka, K.; Marciniak, L. Transition metal ion-based nanocrystalline luminescent thermometry in $SrTiO_3$: Ni^{2+}, Er^{3+} nanocrystals operating in the second optical window of biological tissues. *J. Phys. Chem. C* **2019**, *123*, 18646–18653. [CrossRef]
30. Gharouel, S.; Labrador-Páez, L.; Haro-González, P.; Horchani-Naifer, K.; Férid, M. Fluorescence intensity ratio and lifetime thermometry of praseodymium phosphates for temperature sensing. *J. Lumin.* **2018**, *201*, 372–383. [CrossRef]
31. Rocha, U.; Upendra Kumar, K.; Jacinto, C.; Ramiro, J.; Caamano, A.J.; Garcia Sole, J.; Jaque, D. Nd^{3+} doped LaF_3 nanoparticles as self-monitored photo-thermal agents. *Appl. Phys. Lett.* **2014**, *104*, 053703. [CrossRef]
32. Trannoy, V.; Carneiro Neto, A.N.; Brites, C.D.; Carlos, L.D.; Serier-Brault, H. Engineering of mixed Eu^{3+}/Tb^{3+} metal-organic frameworks luminescent thermometers with tunable sensitivity. *Adv. Opt. Mater.* **2021**, *9*, 2001938. [CrossRef]

33. Pudovkin, M.; Oleynikova, E.; Kiiamov, A.; Cherosov, M.; Gafurov, M. Nd^{3+}, Yb^{3+}: YF_3 Optical Temperature Nanosensors Operating in the Biological Windows. *Materials* **2022**, *16*, 39. [CrossRef] [PubMed]
34. Wei, H.; Cui, F.; Guo, W.; Ye, R.; Lei, L. Nd^{3+}-sensitized NIR downshifting emission in NaYbF4: Nd@NaYF4: Nd nanoparticles for deep tissue temperature sensing. *Opt. Mater.* **2022**, *124*, 112016. [CrossRef]